Carbohydrate Polymers 86 (2011) 1198–1206

Contents lists available at ScienceDirect

Carbohydrate Polymers

journal homepage: www.elsevier.com/locate/carbpol

Nanofibrillated cellulose from Alfa, Eucalyptus and Pine fibres: Preparation, characteristics and reinforcing potential

Iskander Besbes[a], Manuel Rei Vilar[b], Sami Boufi[a,*]

[a] Laboratoire des Sciences des Matériaux et Environnement, Faculté des Sciences de Sfax-Université de Sfax, Tunisia
[b] Université Paris Diderot, Sorbonne Paris Cité, ITODYS, UMR7086 CNRS – F-75205 Paris Cedex 13, France

ARTICLE INFO

Article history:
Received 25 December 2010
Received in revised form 23 May 2011
Accepted 7 June 2011
Available online 16 June 2011

Keywords:
Nanofibril cellulose
Alfa tenassissima
Eucalyptus
Pine
Nanocomposite

ABSTRACT

Cellulose fibres from Alfa (Alfa tenassissima), Eucalyptus and Pine pulp were fibrillated into nanosized fibrils using the homogenization process. To facilitate the fibrillation process, fibres were previously oxidised under neutral conditions to bring the carboxyl content up to 500 μmol/g. Comparison of light transmission and viscosity measurements of the ensuing gels showed that Eucalyptus and Pine fibres were more easily-fibrillated, with a yield in nanosized fibrils exceeding 90% after several passes at 600 bar, than Alfa fibres, which exhibit higher resistance to the fibrillation process. This difference in behaviour was ascribed to the higher crystallinity degree of the Alfa fibres. The morphology of the nanofibrillated cellulose (NFC) from the different fibres using FE-SEM observation revealed nanosized fibrils with widths from 5 to 20 nm, roughly the same for the three types. The reinforcing potential of the ensuing three nanofibrillated cellulose was investigated using dynamic mechanical analysis (DMA) from measurements carried out on nanocomposite films prepared by casting a mixture of NFC suspension and a commercial latex of poly(styrene-co-butyl acrylate).

1. Introduction

During the last decade, there has been a growing interest in the use of nanosized cellulose, namely as a reinforcing phase in polymer based nanocomposites. Their incorporation within a polymer matrix at a level lower than 10% in weight conveys a huge stiffness and mechanical strength (Bhatnagar & Sain, 2005; Fernandes et al., 2009; Zimmermann, Pohler & Geiger, 2004). The high aspect ratio of the nanofibres, their high crystallinity degree, high Young modulus and resistance as well as their aptitude to set up entangled networks stand for a huge improvement of the mechanical properties. Furthermore, given the nanosized effect (nanoscale dimension) of the reinforcement being less than the half of the wavelength of the visible light, high transparency is expected to be obtained.

The application of fibrillated cellulose fibres has been extended to several areas including transparent materials (Abe, Iwamoto & Yano, 2007; Fukuzumi, Saito, Wata, Kumamoto & Isogai, 2009) in packaging applications for their high mechanical properties and low gas permeability rates (Syverud and St enius, 2009), biomedical applications (Czaja, Young, Kawecki & Brown, 2007), production of paper with better sheet properties such as tensile strength (Henriksson, Berglund, Isaksson, Lindstrom, & Nishino, 2009; Sukjoon & Jeffery, 2010). Cellulose nanofibres could also be used as a rheological modifier in foods, paints, cosmetics and pharmaceutical products (Turbak, Snyder & Sandberg 1983), Among the nanosized cellulose fibres, cellulose whiskers, and nanosized fibrillated cellulose (NFC) are the ones that arose the major interest. The former are extracted from fibres after a complete dissolution of the non-crystalline fractions, while the latter results from the high shearing forces of disintegration and the high degree of fibrillation, yielding highly interconnected fibrils with 10–100 nm in width and up to several micrometers in length, depending on the source of cellulose.

The straightforward method to prepare NFC consists to pass a dilute fibre suspension of concentration lower than 1–2 wt% through a mechanical homogenizer (Herrick, Casebier, Hamilton & Sandberg, 1983; Nakagaito & Yano, 2004; Turbak et al., 1983), where a high pressure drop facilitates the nanofibrillation. The procedure can be repeated several times to increase the degree of fibrillation (Abe et al., 2007; Bhatnagar & Sain, 2005). In order to facilitate the fibrillation and reduce the number of passes to lower the energy input, one can combine an additional treatment that may be either physical such as cryocrushing (Alemdar & Sain, 2008), ultrasonication (Johnson, Zink-Sharp, Renneckar & Glasser, 2009) or chemical, such as controlled oxidation (Habibi, Mahrouz

* Corresponding author.
E-mail address: sami.boufi@fss.rnu.tn (S. Boufi).

0144-8617/$ – see front matter © 2011 Elsevier Ltd. All rights reserved.
doi:10.1016/j.carbpol.2011.06.015

& Vignon, 2009; Saito & Isogai, 2004; Saito, Nishiyama, Putaux, Vignon & Isogai, 2006; Saito, Hirota, Tamura, Kimura, Fukuzumi, Heux & Isogai, 2009). Enzyme-treatment was also found to facilitate fibrillation, and the nanofibers produced undergo lower degradation effects (Henriksson, Henriksson, Berglund & Lindström, 2007; Pääkkö et al., 2007).

The main sources of cellulose fibres are annual plants and wood with its two species namely hardwoods and softwoods. They are organized in a cellular hierarchical structure build up by bundles of thin microfibrils aggregated into larger structures embedded into hemicellulose and enclosed by lignin. The typical cross section of the microfibrils ranges from 4 to 20 nm depending on their origin, and each of them is formed by the association of many cellulose molecules, which are linked together in repeating lengths along their chains (Fengel, 1971). Wide differences in the anatomical features and ultrastructure characteristics exist between the different sources of cellulose fibres, such as the microfibril angle of the different layers, particularly those in the secondary wall, the amount of hemicellulose and the size of the microfibrils (McDougall, Morisson, Stewart, Weyers & Hillman, 1993). These differences are likely to affect the characteristics of the NFC produced. Wolfgang and Sanadi (2009) showed that fibrillation proceeds much faster and more easily for the pulp fibres of softwood relatively to hardwood. Moreover, the mechanical properties of cellulose films from nanofibres displayed a lower strength for hardwood but a slightly higher modulus for softwood. The effect of hemicelluloses, as matrix substances on the nanofibrillation process using a grinder treatment, was analysed by Iwamoto, Abe, and Yano (2008). The variation of the treatment procedure to extract lignin and the post drying of the pulp showed that hemicelluloses play an important role in facilitating nanofibrillation, as well as improving the thermal and mechanical properties of the nanocomposites.

In a previous study, we showed that TEMPO oxidation of dried softwood pulp up to a critical level facilitated the defibrillation process (Besbes, Alila & Boufi, 2011), reduced the number of passes necessary to get the gel and prevented the clogging of the homogenizer. These effects became apparent up to a carboxyl content about 300 μmol/g, and over 500 μmol/g the yield in the nanoscale fibrillated cellulose exceeded 90%, namely at a defibrillation pressure of 600 bar. In the present work, we adopted the same procedure to prepare NFC from three different sources of fibres, namely Alfa fibres, softwood and hardwood. The ease of fibrillation will be analysed according to the cellulose origin and the morphological aspect of the ensuing nanofibrillated material. The reinforcing potential of the different NFC and the optical characteristic of a nanocomposite film obtained by casting a mixture of NFC and acrylic polymer latex will also be analysed.

2. Experimental

2.1. Materials

Commercial bleached Eucalyptus pulp (Eucalyptus globulus) and Pine (Pinus sylvestris), in the dry form, were used as starting material for the preparation of NFC. 2,2,6,6-tetramethylpiperidine-1-oxyl radical (TEMPO), sodium bromide (NaBr), sodium hypochlorite solution (NaClO), sodium chlorite ($NaClO_2$) were purchased from Sigma–Aldrich and used as received without further purification.

2.2. Preparation of Alfa fibres

Alfa fibres also called esparto grass (Stipa tenacissima L.) are gray-green needlegrasses growing abundantly in the arid steppes of central Tunisia were collected at Khassirne in the middle of Tunisia. They were cut to the length of 2–3 cm and cooked in a digester with an aqueous solution of NaOH (15% in volume) at a maximum temperature of 160 °C. The ensuing pulp was washed three times with water and submitted to a bleaching treatment to remove the residual lignin. A three stage bleaching was accomplished according to the conditions reported in Table 1.

Table 1
Bleaching conditions of Alfa pulp.

Stage	D1	*E*	D2
Chemical charge	$NaClO_2$ (3%) Acetic acid (2%)	NaOH (5%)	$NaClO_2$ (3%) Acetic acid (2%)
Pulp consistency	5%	5%	5%
Temperature	70 °C	70 °C	70 °C
Time	180 min	120 min	180 min

2.3. Fibres morphology

The fibres morphology was determined using MorFI (LB-01) analyser. The technique is based on the image analysis of a diluted suspension of fibres with a CCD video-camera.

2.4. TEMPO-mediated oxidation

The TEMPO-mediated oxidation was carried under neutral condition according to the method reported by Saito et al. (2009). Cellulose fibres (5 g) were dispersed in 0.05 M sodium phosphate buffer (500 mL, pH 7) solution, containing TEMPO (25 mg) and NaBr (250 mg). Sodium chlorite (1.13 g, 10 mM) solution and sodium hypochlorite solution (0.5 ml of 2 M solution, 1.0 mM) were added at a first step to a flask. The mixture was then stirred at 500 rpm and 60 °C for fixed periods of time going from 2 to 4 h, according to the fibres origin. During the oxidation process, the coloration of the mixture turned into yellow owing to the generation of free chlorine. The oxidation was stopped by adding 100 mL of ethanol, and the oxidised fibres were filtered and washed two times. After cooling the suspension to room temperature, the oxidised celluloses were thoroughly washed with water and then filtrated.

2.5. Carboxyl content

The carboxyl contents of the oxidised celluloses were determined using conductometric titration. The wet fibre (50–100 mg) was suspended in 15 mL of a 0.01 M HCL solution to exchange the sodium cations bound to the carboxyl groups by hydrogen ions. When a stable suspension was obtained, the mixture was titrated with a 0.01 M NaOH solution. The titration curves showed the presence of a strong acid corresponding to the excess of HCl and a weak acid corresponding to the carboxyl content. The total amount of carboxyl groups was calculated from:

$$C = (V_1 - V_0) \times C_{NaOH} \quad (1)$$

being C the carboxyl concentration, V_1 and V_0 the equivalent volumes of added NaOH solution, C_{NaOH} the exact concentration of NaOH solution and m, the weight of the dried product.

2.6. Fibrillation process

The fibres were dispersed in water with a concentration of 1–2 wt% and then homogenized by different passes through a high pressure homogenizer (NS1001L PANDA 2K-GEA), operated at a pressure ranging from 100 to 1000 bar and at an operating temperature between 60 ° and 70 °C, until a translucent gel is obtained. Unless specified, pH of the fibres suspension was neutral.

2.7. Yield in nanofibrillated cellulose

A diluted suspension with about 0.2–0.1% of solid content was centrifuged at 4500 rpm for 20 min to separate the nanofibrillated material (in supernatant fraction) from the non-fibrillated and the partially fibrillated ones, which sedimented down, before being dried to a constant weight at 90 °C in a halogen desiccator. The yield was calculated from:

$$\text{Yield\%} = \left(1 - \frac{\text{weight of dried sediment}}{(\text{weight of diluted sample} \times \%\text{Sc})}\right) \times 100 \quad (2)$$

The results represent the average values of the three replications.

2.8. Nanocomposites processing

A commercial latex (PROKIL S330P-MPC-PROKIM-Tunisia) obtained by the copolymerization of styrene (34 wt%) and butyl acrylate (64 wt%), and containing 1 wt% acrylic acid and 1 wt% acrylamide, was used as a matrix. The size of the polymer particles is around 140 nm and the solid content is 50 wt%. The glass–rubber transition temperature (T_g) of the poly(S-co-BuA) copolymer was about 25 °C.

The NFC gel (solid fraction 1–2 wt%) were mixed with the latex in various amounts in order to obtained from oxidized fibres with carboxyl content of 500 μmol/g and 5 passes at 300 bar followed by additional 10 passes at 600 bar composite films with weight fraction of cellulose ranging from 0% to 15%. After stirring the latex and the NFC suspension for 1 h, the mixture was cast in a TEFLON mould and stored at 40 °C until complete water evaporation and polymer particle coalescence. A transparent to translucent film was obtained according to the NFC content, with a thickness in the range of 300–400 μm.

2.9. Diffraction analysis

The crystallinity index (CrI) of cellulose was calculated from an X-ray diffraction (DRX) pattern obtained using a Bruker AXS diffractometer (Bruker AXS, Madison, WI) with a Cu Kα radiation, generated at 30 kV and an incident current of 100 mA, incident on small pieces of the nanofibres suspension after dried in the air. The (2θ) angular region from 5° to 50° was scanned with steps of 0.05° and a step time of 10 s. CrI was calculated using the intensity values corresponding to the diffraction of the crystalline structure and the amorphous fraction, according to the Segal method (Segal, Creely, Martin & Conrad, 1959):

$$\text{CrI\%} = \left[\frac{I_{200} - I_{am}}{I_{200}}\right] \times 100 \quad (3)$$

I_{200} is the intensity of the crystalline peak at the maximum at 2θ between 22° and 23° and I_{am} is the intensity at the minimum at 2θ between 18° and 19°. Eq. (3) can be used to compare the CrI of samples from the different types of fibres, prepared following analogous protocols.

2.10. Field-emission scanning electron microscopy (FE-SEM)

Field emission scanning electron microscope (FE-SEM) images were obtained with a ZEISS SUPRA40 fully controlled from a computer workstation. The electron source, a hot cathode producing electrons by Schottky effect, is a tungsten filament coated with a ZrO layer. Images are created by the software SMARTSEM. A drop of the NFC suspension, with a solid content about 0.2–0.5%, was deposited and dried on a silicon wafer and coated with a thin carbon layer applied by sputtering with a thickness limited to 3 nm.

2.11. Transmittance measurements

NFC suspensions (0.1% loading) were introduced into quartz cuvettes and the transmittance was measured between 400 and 800 nm using a Shimadzu UV–Vis spectrophotometer. The spectrum of a cuvette filled with water was used as blank.

2.12. Dynamic mechanical analysis (DMA)

Dynamic mechanical analysis (DMA) experiments were conducted in tension mode using a PYRIS™ Diamond DMA (Perkin-Elmer, Waltham, MA, USA). Temperature scans were run from −50 °C up to 100 °C at a heating rate of 2 °C/min, a frequency of 1 Hz and an amplitude of 10 μm. The storage (E') and the loss (E'') *moduli*, as well as the loss factor $\tan\delta = (E''/E')$, were measured as a function of the temperature. Sample dimensions were about 20 mm (length), 10 mm (width) and 0.3–0.5 mm (thickness).

2.13. Raman Spectra

Raman spectra were collected on a LabRAM Analytical Raman micro-spectrograph (Jobin-Yvon, Horiba group, France) using a He-Ne laser source as exciting radiation ($\lambda = 632.8$ nm) and an air-cooled CDD detector. The samples were in the form of a dry sheet.

3. Results and discussion

3.1. Nanofibrillation of oxidized fibres

In a previous study, (Besbes et al., 2011), it was shown that a TEMPO-oxidation of cellulose fibres significantly reduces the number of passes necessary to bring about the nanofibrillation. It was also shown that the carboxyl content is an essential parameter in determining the yield of fibrillation and the transparency degree of the ensuing gel. With these bases, and to reduce the fibrillation of the cellulose fibres at a minimum number of passes using the homogenization process, the three types of fibres here analysed were oxidised to increase the carboxyl concentration up to 500 ± 30 μmol/g. It was postulated that the ease of fibrillation has results of concomitant effects: (i) the oxidation generates negative charges that bring forth repulsive forces between microfibrils (Saito et al., 2006) within the cell wall, contributing to loosen the microfibrils cohesion held by hydrogen bonding; (ii) the oxidation favours the hydration and the swelling of the fibres, making them more flexible and the crystalline zone more accessible; (iii) the oxidation loosens the primary S1 cell wall making the S2 layer more reachable and more prone to fibrillation during the homogenization process; (iv) finally, the oxidation results in chain scission in the amorphous zone, creating defaults within the fibre cell wall, which facilitates the mechanical fibrillation.

From Fig. 1 and Table 2, one can see that the number of passes necessary to reach the gel aspect is roughly the same for the three types of fibres, despite the important difference in their respective lengths. However, the yield of nanofibrillation depends notably on the homogenization pressure, as well as on the fibres origin. In all instances, the highest yield is attained with Eucalyptus fibres, which reaches 65% at 300 bar and after 5 passes. Comparatively, in the same conditions, the yield attained for Alfa and Pine is 28% and 42%, respectively. Additional 10 passes at a pressure of 600 bar bring about a notable improvement in the fibrillation yield for Eucalyptus and Pine fibres, attaining 96% and 88%, respectively. However, only a fairly small improvement is noted for Alfa fibres with fibrillation yields lower than 50%. Further passes at 600 bar do not bring substantial increase on the fibrillation yield. One could ask about the remarkable lower fibrillation yield of the Alfa fibres compared to those of Eucalyptus and Pine, a sign of a higher difficulty to break

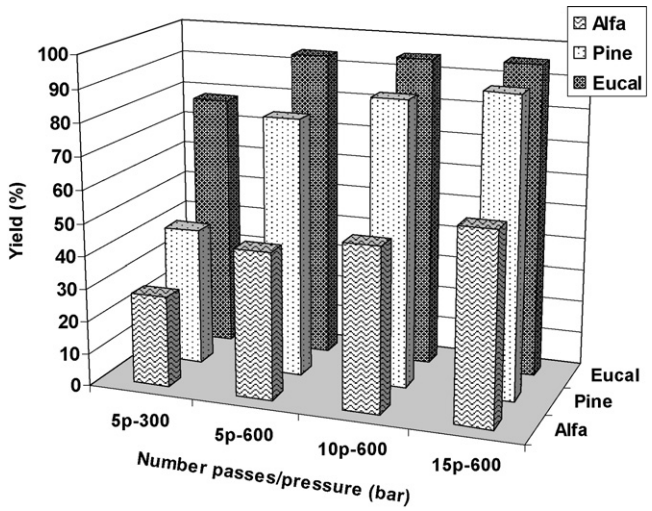

Fig. 1. Yield in nanofibres of different origins (Alfa, Eucalyptus and Pine) vs. the number of passes and the homogenization pressure.

down the cohesion of the fibres aggregation within the cell wall to release the microfibrils. Different parameters may affect the ease of fibrillation, among which, one can cite the crystallinity index, the chemical composition, namely the cellulose/hemicellulose/lignin ratio and the morphological properties (length and width). Comparative analyses of these parameters for the present fibres were carried out to account for these differences.

With regard to the morphological properties of the fibres, one can rule out this parameter, considering that the length and width of the Pine fibres were about two times higher than those of Alfa and Eucalyptus at the moment where their fibrillation behaviour is similar to that of Eucalyptus (Table 2).

Raman spectroscopy can be successfully used to rapidly evaluate the chemical composition of lignocellulosic compounds (Agarwal, 1999), in terms of the proportion of cellulose, hemicellulose and lignin. This technique has the significant advantages of not requiring sample preparation. Moreover, it is not sensitive to the humidity degree of the samples and is a non-destructive method. In Raman spectra, the vibrational mode associated with (C–O–C) of the β-(1–4) glycosidic linkages of the glucopyranose units at 1120 cm^{-1} corresponding to the symetrical stretching (v_s), encompasses both cellulosic and non-cellulosic carbohydrate (hemicellulose). In contrast, the band at 1098 cm^{-1}, assigned to the asymmetric (C-O-C) stretching mode, is not influenced by hemicellulose (Agarwal, Atalla & Forsskåhl,1995; Edwards, Farwell & Webster 1997). Therefore, the ratio R given by Eq. (4) and corresponding to the ratio of the intensity of the symmetric and that of the asymmetric stretching mode:

$$R = \frac{Iv_s(C-O-C)}{Iv_{as}(C-O-C)} \quad (4)$$

Table 2
Morphological properties of cellulose fibres used for the extraction of NFC and yield in nanofibres at 300 and 600 bar.

	Alfa	Eucalyptus	Pine
Carboxyl content (μmol/g)	500	510	500
Mean fibre length (mm)[a]	0.72	0.87	1.85
Mean fibre diameter (μm)[a]	20	28	33
	20	27	34
Number of passes to attain the gel[b]	6	5	5
Yield after 5 passes at 300 bar in (%)	28	65	42
Yield after 10 passes at 600 bar in (%)	50	96	88

[a] Parameters determined from MorFI analysis.
[b] Pressure being maintained constant at 300 bar.

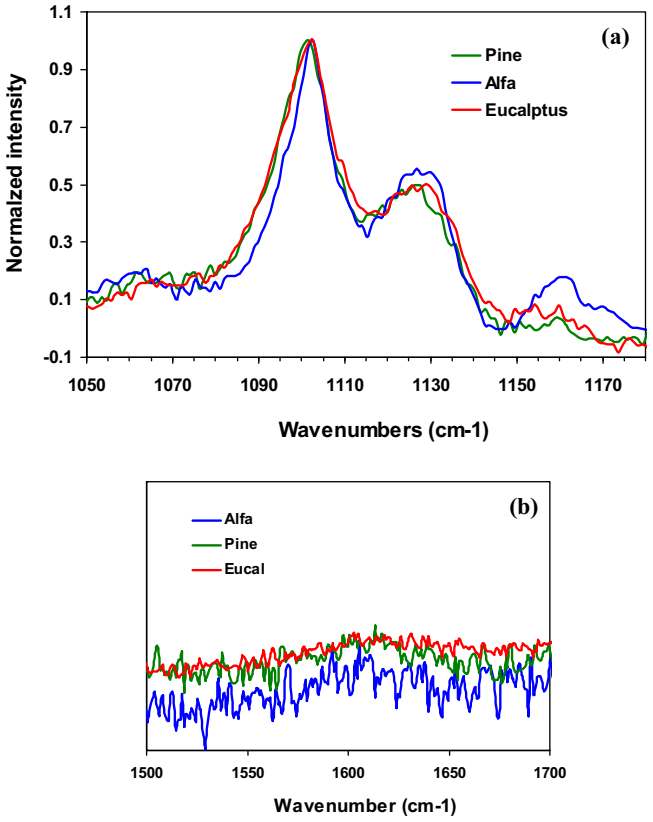

Fig. 2. Raman spectra of Eucal-500, Alfa-500 and Pine-500 fibres in the (a) 900–1200 cm^{-1}, and (b) 1500–1700 cm^{-1} range.

can be used as an indicative parameter of the hemicellulose content. From Fig. 2a, showing the typical v_{as} and v_s bands of the C–O–C, one could deduce that the hemicellulose content on the three types of fibres is roughly the same and could not account for the difference in the fibrillation behaviour during the homogenization process. Conversely, the absence of any band in the region 1600–1700 cm^{-1} (Fig. 2b) confirmed the complete removal of lignine from the fibres after the bleaching and oxidation treatment. Indeed, residual lignine, likely to be present on the fibres, can be readily detected by Raman spectroscopy through the strong band at 1600 cm^{-1} assigned to the aromatic ring stretching mode.

However, if the DRX patterns of the oxidised fibres (Fig. 3) are compared, it can be observed that the Alfa fibres exhibit a higher

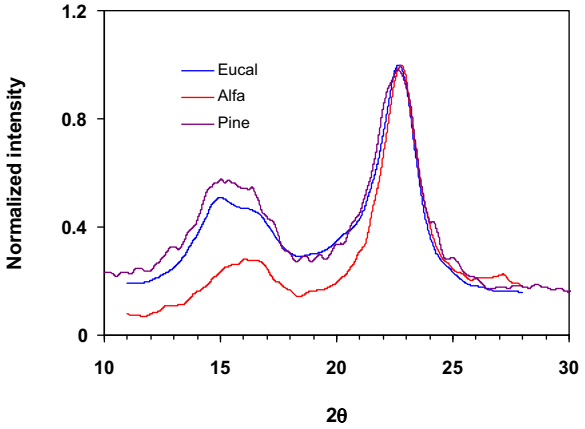

Fig. 3. Normalized XRD patterns of oxidized fibres of Eucalyptus, Alfa and Pine.

crystallinity index than those of Eucalyptus and Pine fibres. The crystalline index, calculated according to Eq. (1), is about 92, 86 and 87% for Alfa, Eucalyptus and Pine fibres, respectively. Since the analysis conditions for the DRX measurement were the same, therefore the CrI could be used to compare the trend in the crystallinity of the fibres. Therefore, it can be inferred that the higher crystalline degree of Alfa fibres accounts for the harder fibrillation aptitude by the high pressure homogenizer. This hypothesis is plausible if the fibres are considered as being composed of cellulose microfibrils aggregated into larger structures embedded into hemicellulose with imperfect axial orientation and less ordered interlinking regions between the crystallites inside the elementary fibrils. These zones constitute the locus of the amorphous region, being the weakest ones from which the fibrillation starts. It is worthy noting that the CrI value for oxidized eucalyptus pulp is faintly higher than one reported in literature (Roncero, Torres, Colom, & Vidal, 2003), which is in the range of 80–84%. The higher value is likely the result of the oxidation treatment, which removes a part of hemicellulose. One also should not exclude overestimation of the crystalline degree owing to the method used. Indeed, as pointed by Thygesen, Oddershede, Lilholt, Thomsen, and Ståhl (2005), the Segal method for the CrI calculation gives usually higher value than other methods.

3.2. Optical aspect

The appearance of the ensuing NFC gel (at 1.5% solid content and without any dilution) issuing from the different fibres, as a function of the number of passes is shown in Fig. 4. For all the samples, a translucent gel, whose transparency degree differs according to their origin and the number of passes, is obtained. After several passes (4–7) at 300 bar, the transparency degree of the gel was quite low, namely the one from Alfa fibres. On the other hand, contrarily to NFC from Alfa, a significant improvement in the transparency degree is observed in the gel after additional passes at 600 bar for the samples issuing from Eucalyptus and Pine fibres (see: Fig. 4: Eucalyptus and Pine from I to III).

Further evidence of the effect of the homogenization condition on the transparency of the NFC suspension is depicted from UV–Vis transmittance spectra of a diluted suspension (Fig. 5). As previously observed, for the samples homogenized at 300 bar and after 5–6 passes, the lowest transmittance is noted for Alfa fibres followed by Eucalyptus and Pine. A huge increase in transmittance is achieved after 5–10 additional passes at 600 bar, with a more pronounced effect for Pine followed by Eucalyptus. Increasing the number of passes to 15 did not further enhance the transparency degree, as confirmed by the fair shift of the transmittance to higher values compared to that of samples issued from 10 passes.

The transmittance curve from 400 to 800 nm is a simple mean to get a rough idea about the width of the ensuing fibrils and the extent of the nanofibrillation of the fibres. In fact when light passes through a medium containing randomly dispersed particles, it is scattered by the particles causing a reduction in the transparency degree. Scattering is brought by discontinuities in refractive index and encompasses mainly two scattering types, namely Rayleigh scattering and Tyndall scattering or Mie scattering (for spherical particles). The former scattering mode is predominant from tiny particles being lower than 1/10 wavelength (about 40 nm) and its magnitude has a very strong dependence on the size of the particles and on wavelength of light. While the later scattering prevails for particle sizes larger than a wavelength with intensity being interdependent on the wavelength, but is sensitive to the particle size. In the present case, the nanofibrillated cellulose with width lower than 40 nm will be involved in Rayleigh scattering and accounts for the wavelength-dependence of the transmittance (lower transmittance in the shorter wavelength). On the other hand, as the Tyndall scattering intensity is proportional to the third power of particle size, the non-fibrillated fraction is responsible on the huge decrease of the transparency of the ensuing gel. This explains the trend in the evolution of the transparency or the transmittance of the NFC for the different origin: the higher the non-fibrillated fraction, the more of the light is scattered and the less transparent is the ensuing NFC gel. The higher transmittance with additional passes at a higher pressure means a decrease in the amount of non-fibrillated and partially fibrillated fractions responsible for light-scattering phenomenon.

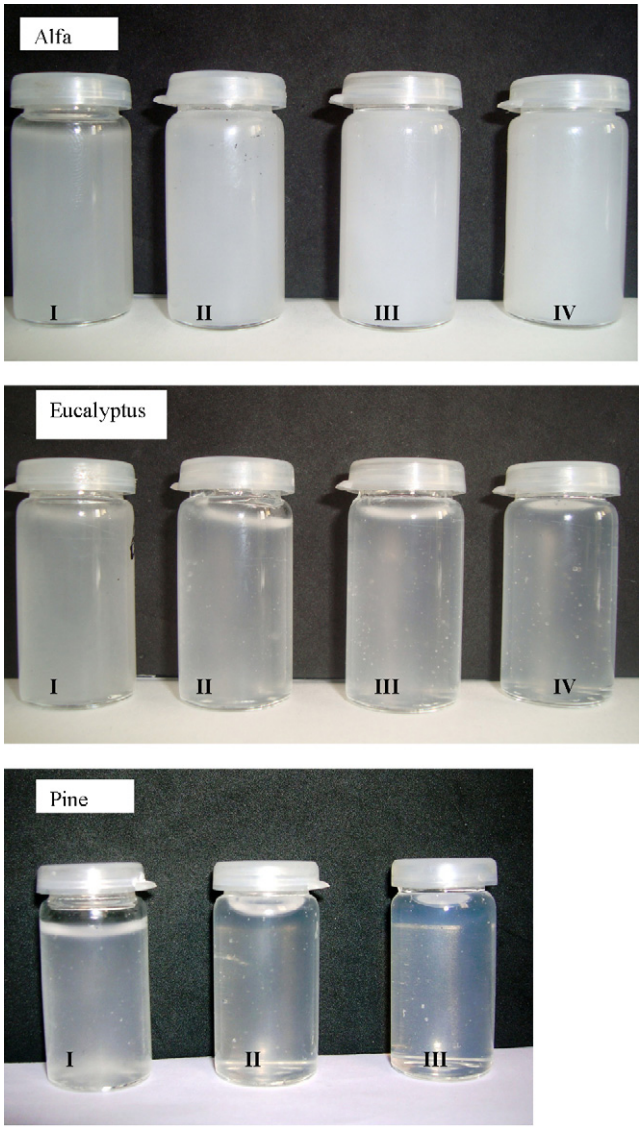

Fig. 4. Appearance of NFC gel at 1.5 wt% issuing from; Alfa, Eucalyptus and Pine fibres after (I) 5 passes at 300 bar, (II) 5 additional passes at 600 bar, (III) 10 additional passes at 600 bar and (IV) 15 additional passes at 600 bar.

In addition to the nanoscale size of the fibrillated cellulose, thorough colloidal stability is prerequisite for good transparency of the NFC gel. In the present case, this stabilization is ensured through the ionized carboxylic groups providing electrostatic stabilization. The key rule of carboxylic groups could be highlighted by analysing the transmittance evolution with pH. Indeed, as shown in Fig. 5b, a huge downward shift of the transmittance occurred as the NFC pH suspension is lowered to 3. This phenomenon is likely the consequence of a change in the dissociation degree of the carboxylic groups, being mainly in the form of –COO– over pH 6, while they are undissociated beneath pH 4.

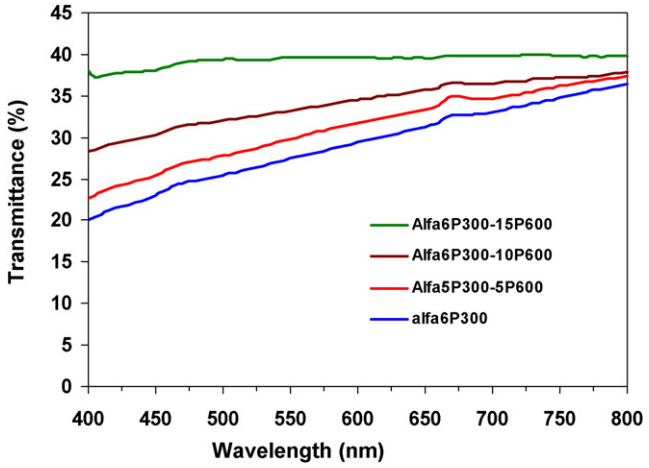

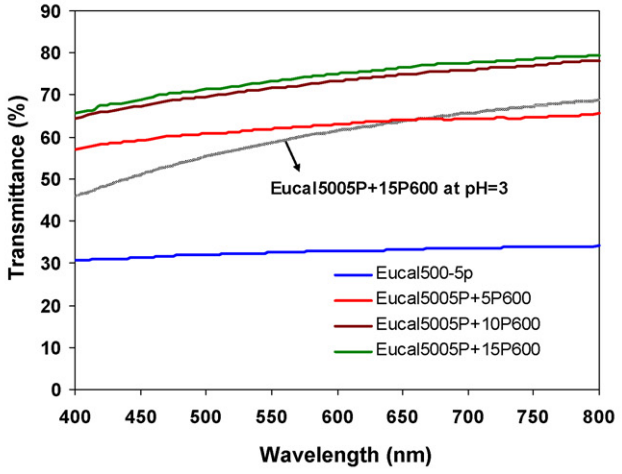

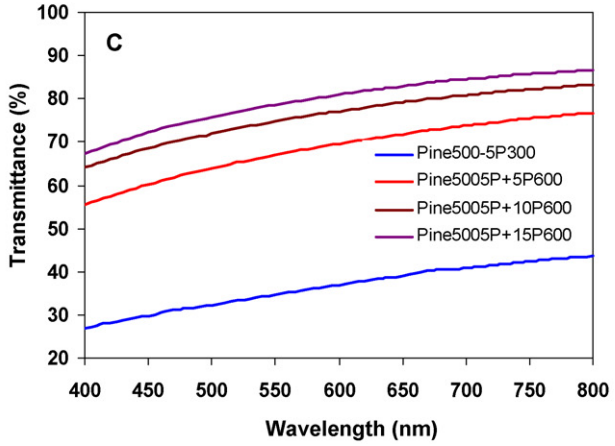

Fig. 5. UV–Vis transmittance spectra of the NFC suspension (without any centrifugation) from Alfa, Eucalyptus and Pine fibres after 5 passes at 300 bar and additional passes at 600 bar: concentration was of 0.1 wt% with a 1 cm path length.

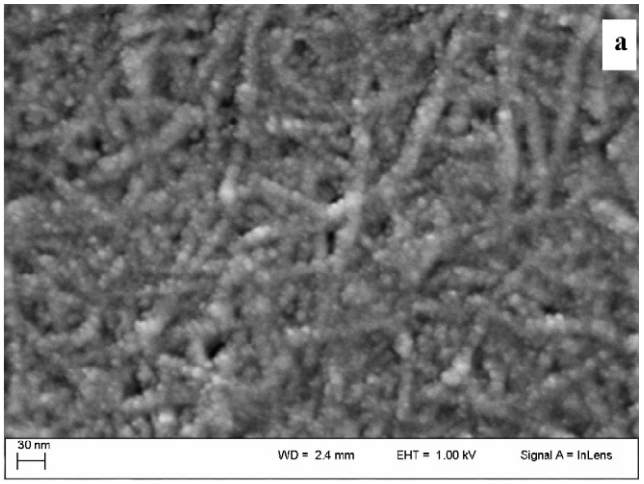

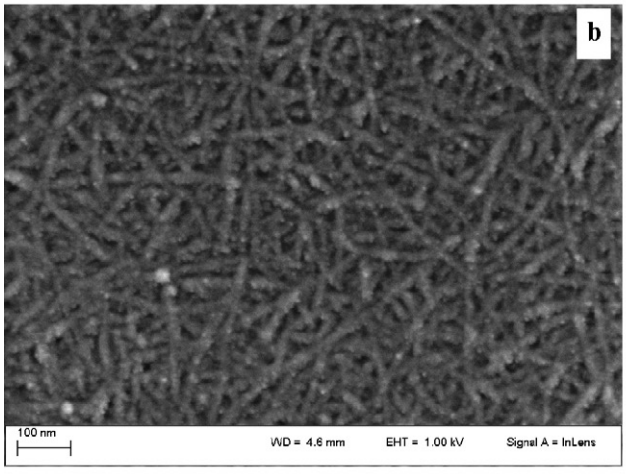

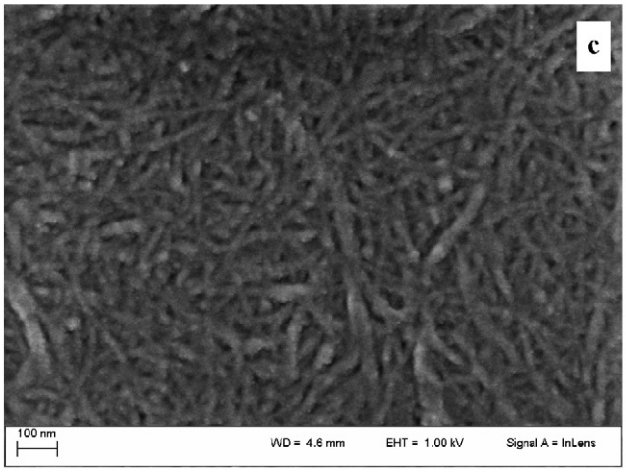

Fig. 6. FE-SEM images of the supernatant fraction of high-pressure homogenized fibres after 5 passes at 300 bar; (a) Pine, (b) Eucalyptus and (c) Alfa fibres.

3.3. Morphology of NFC

To get a more accurate idea about the dimension scale of the prepared NFC, FE-SEM observations were carried out on samples obtained by depositing a drop of the supernatant fraction of the NFC suspension (with a solid content between 0.2 and 0.1%) on a silicon wafer. To avoid damaging the samples during the analysis, the acceleration voltage was maintained at a relatively low range (0.5–1 kV).

FE-SEM images of NFC from Alfa, Eucalyptus and Pine are shown in Fig. 6. All of the supernatant fractions of the ensuing NFC showed nanosized fibrils with widths ranging between 5 and 20 nm, which seems to be roughly the same for the three NFC types. Further passes at higher pressure i.e. 600 bar did not modify the width of the fibrils, which could be an indication that the nanosized fibrils on the supernatant fraction really correspond to the ultimate microfibril building up of the fibres.

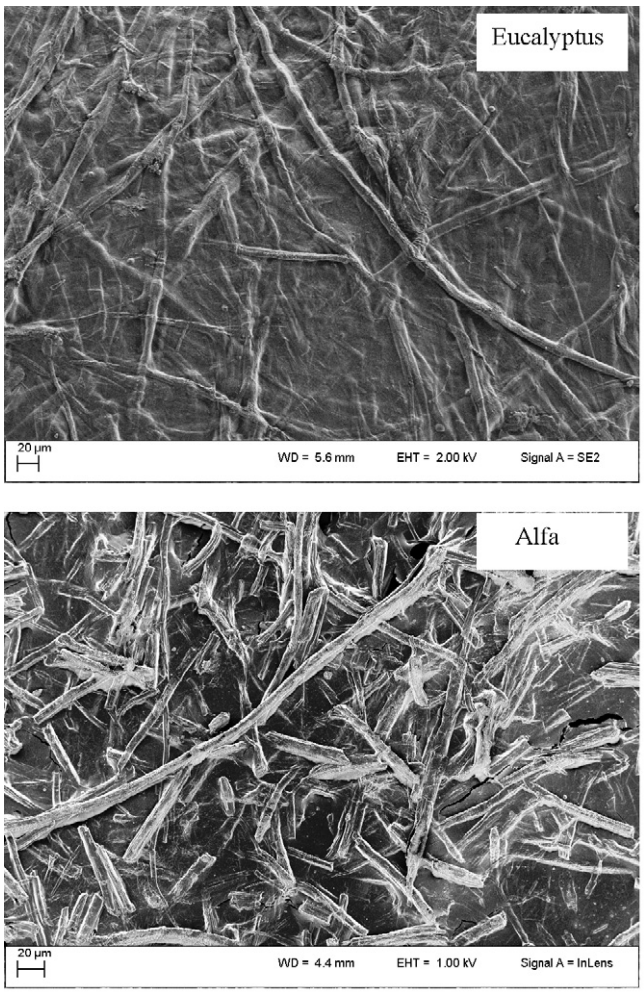

Fig. 7. FE-SEM images of the sediment fraction.

Based on the line width of the peak from crystalline plane 200 and using the Scherrer Equation (Langford & Wilson, 1978), the lateral width of the crystallites in the fibres used as raw material was between 6 and 8 nm. The higher value of the width noted from the FE-SEM observation may arouse from the coating layer of carbon applied on the samples, whose thickness is estimated to be about 4–5 nm. This layer, applied by sputtering, helps to increase surface electrical conductivity and consequently, to avoid charging effects and improve the image resolution.

The examination of the morphology of the sediment fraction of the NFC presented in Fig. 7 reveals fibres with widths between 2 and 20 μm and lengths exceeding 500 μm. Higher magnification shows an aggregated structure of microfibrils, forming a highly entangled web-like layer. These microfibrils were released and individualized after passing through the homogenizer, where high shearing forces break down the physical cohesion of the fibrils.

3.4. DRX analyses

The crystalline degree of the ensuing NFC compared to the original fibres was also evaluated from Wide Angle X-Ray Scattering (WAXS) measurements using Eq. (3). NFC samples did not exhibit any evolution in their polymorph type. However, as shown in Table 3, their CrI decreased with the fibrillation action, the most important effect being observed for Eucalyptus fibres. The drop in the crystallinity index is amplified by the number of passes and the fibrillation pressure.

Table 3
Evolution of the CrI after fibrillation at 300 and 600 bar.

	Pristine	5p-300 bar	5p-600 bar	10p-600 bar
Alfa	92		90	85
Eucalyptus	86	83	71	66
Pine	87	81	79	75

3.5. Dynamic mechanical analyses (DMA) of the nanocomposite film

To compare the reinforcement potential of the three NFC, DMA measurements were carried out on nancomposite films cast on a teflon mould from an aqueous suspension of cellulose microfibrils and a commercial latex of poly(styrene-co-butyl acrylate). The temperature dependence of the storage tensile modulus E' and at 1 Hz for the unfilled poly(S-co-EHA) matrix with different MPS contents is shown in Fig. 8. For the seek of a better clarity, E' curves were normalized at 1 GPa at low temperature i.e.; below −10 °C. This was also justified by the low reinforcing effect of nanofiller beneath the glass transition of the matrix.

In the rubbery region, an important reinforcing effect was noted by the addition of NFC irrespective of their type, which is in accordance with the well-recognized reinforcing potential of nanofibrillated cellulose.

In order to compare the stiffening effect of the three NFC, the evolution of the storage modulus E' for the nanocomposite film measured at 60 °C, i.e. around the T_g value + 40 °C, vs. the NFC loading is plotted in Fig. 9. The continuous rise of the same trend in the relative modulus clearly confirms the strong reinforcing potential of the as-prepared NFC sample. For instance, as the NFC loading reached 4 wt% (corresponding to 2.7 vol%) the modulus of the nanocomposite increased by almost two orders of magnitude compared with that of the neat matrix. This high reinforcing effect is attributed to the formation of a stiff percolating nanofibrils network linked by strong hydrogen bonds between adjacent nanofibres (Azizi Samir, Alloin, Paillet, & Dufresne, 2004; Malainine, Mahrouz & Dufresne, 2005). Above a critical level, this reinforcement is common to cellulose-based nanofiller, and is credited to the formation of a stiff percolation network, the percolation threshold (ϕ_p) can be determined by applying a power law function to the E' vs. NFC loading according to Eq. (5) as predicted from the percolation theory (Gouyet, 1992)

$$E' \propto \left(\frac{\phi - \phi_p}{1 - \phi_p}\right)^b \quad \text{For } \phi > \phi_p \tag{5}$$

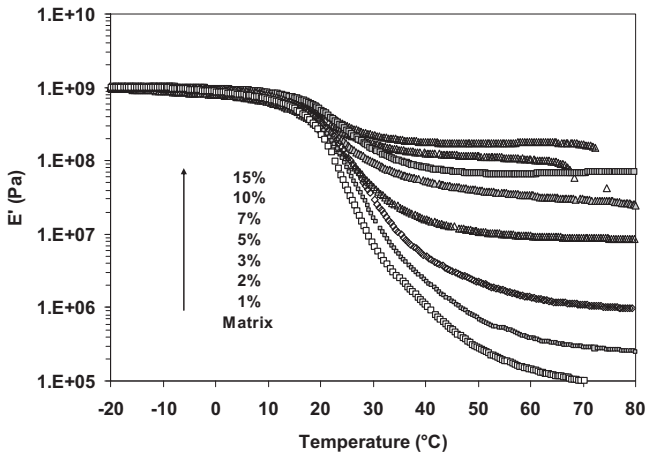

Fig. 8. Evolution of the storage tensile modulus E' vs. Temperature at 1 Hz for nanocomposite film prepared from Eucal-500 NFC and acrylic latex.

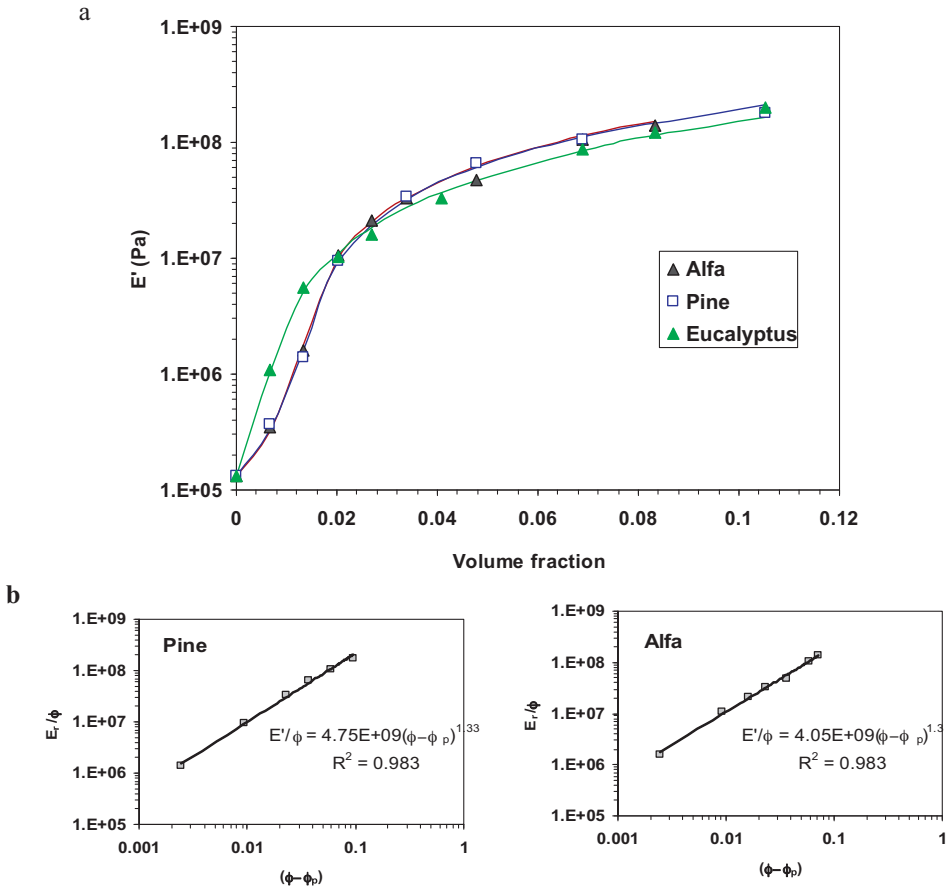

Fig. 9. Evolution of the storage modulus at 60 °C vs. volume fraction of NFC for nanocomposite film prepared from Eucalyptus, Pine and Alfa fibres and acrylic latex: comparison between the experimental data (the symbols), and one predicted from the percolation approach.

Applying this concept for the three NFC type, the percolation threshold was adjusted to the value, which gives the best linear regression for E' vs. $\left(\frac{\phi-\phi_p}{1-\phi_p}\right)$ on a log–log scale. The results collected from this analysis are presented in Table 4.

It can be seen from Fig. 9 that the simulated value of the modulus, obtained from the percolation, approach were in good agreement with the experimental data from DMTA measurement. The E' values were calculated from the percolation approach (Ouali, Cavaillé & Perez, 1991) according to the following equation:

$$E_c = \frac{(1-2\psi+\psi\phi)E_sE_r + (1-\phi)\psi E_r^2}{(1-\phi)E_r + (\phi-\psi)E_s} \quad (6)$$

where ψ can be written as:

$$\psi = 0 \quad \text{For} \quad \phi \geq \phi_p \quad (7)$$

$$\psi = \left(\frac{\phi-\phi_p}{1-\phi_p}\right)^b \quad \text{For} \quad \phi \geq \phi_p \quad (8)$$

Table 4
Percolation threshold for the nanocomposite prepared from Alfa, Eucalyptus and pine NFC obtained after 5 passes at 300 bar.

	ϕ_p	b	R^2
Alfa	0.013	1.3	0.996
Eucalyptus	0.0035	1.5	0.998
Pine	0.01	1.35	0.995

ψ and ϕ are the volume fraction of percolated structure and the total volume fraction of the nanofiller, respectively. E_s and E_r are the modulus of the cellulose network and of the matrix respectively. The modulus of the cellulose network E_r used for the calculation was set 5 GPa based on reported bibliographic data (Dalmas, Cavaillé, Gauthier, Chazeau & Dendievel, 2007).

From Table 4, one can see that NFC from Eucalyptus exhibited much lower percolation threshold compared to the ones of Alfa and Pine fibres (0.3 vol% for Eucalyptus NFC against 1.3 and 1.0 vol% for Alfa and Eucalyptus, respectively). The lower value of the former may be explained by the much higher yield in nanofibrillated material. Further, if we consider nanocomposite based on cellulose whiskers with an aspect ratio 50, then the percolation threshold attained about 1.4 vol%, to a large extent higher than the one reached for NFC from Eucalyptus. The huge difference might be rationalized to the higher length of NFC and their ability to gives rise to entangled network. Indeed, it is well reported that the percolation threshold is inversely proportional to the aspect ratio (De Gennes, 1976) of the dispersed particles. Work is in progress for the analysis of the evolution of the percolation threshold after further fibrillation at 600 bar for Pine fibres.

Moreover, despite the difference in the fibrillation yield between Eucalyptus, Alfa and Pine fibres, it can be noted from Fig. 9 that the dependence E' on the NFC loading, beyond the percolation threshold, follows roughly the same trend for the three NFC, irrespectively of their origin. In other words, NFC issuing from Alfa, Eucalyptus and Pine fibres exhibit the same reinforcing potential, above 1 vol%, despite the difference in their yield in nanofibrillated material. However, attention should also be drawn to the

mechanical strength of the film, which is the subject of an ongoing work.

4. Conclusion

Cellulose nanofibres with diameter ranging from 5 to 20 nm were isolated from three different sources of fibres viz; Alfa, Eucalyptus and Pine. A TEMPO-oxidation treatment at neutral conditions was carried out on the fibres to increase the carboxyl content up to 500 μmol/g in order to facilitate the fibrillation process during the high pressure homogenization. Although, a consistent gel could be obtained after 5–6 passes at 300 bar for all the fibres: the yield in nanofibrillated material is the lowest for Alfa fibres and did not grow significantly with further passes for higher pressures. Besides, a yield higher than 90% was obtained with Eucalyptus fibres after 5 passes at 300 bar, followed by 5 additional passes at 600 bar. FE-SEM observation confirmed the nanosized scale of NFC with a width being contained in the range of 5–20 nm for the different samples.

The incorporation of the ensuing NFC into a polymer matrix, up to 15 wt% loading, imparted a high reinforcing effect, confirmed by a huge enhancement in the tensile modulus of the nanocomposite film. This well-known effect is ascribed to the formation of a stiff percolating nanofibrils network held by a strong hydrogen bonding between adjacent nanofibres.

In spite of the important difference in the yield of nanofibrillated material issuing from the different fibres, the evolution of E' vs. NFC loading follows the same trend. Research is in progress to analyse the effect of the NFC addition in the tensile strength of nanocomposite films.

Acknowledgments

The authors owe an utmost thank for the NATO (grant NATO062010-CBP.MD. CLG983981) and the Tunisian Ministry of Higher Education and Scientific Research for their financial support. They also extend their gratitude to Mr. Frédéric Herbst for his contribution in the FE-SEM images and to USC "Raman" for the raman spectra.

References

Alemdar, A., & Sain, M. (2008). Isolation and characterization of nanofibers from agricultural residues – Wheat straw and soy hulls. *Bioresource Technology*, *99*, 1664–1671.

Abe, K., Iwamoto, S., & Yano, H. (2007). Obtaining cellulose nanofibers with a uniform width of 15 nm from wood. *Biomacromolecules*, *9*(3), 1022–1026.

Agarwal, U. P., Atalla, R. H., & Forsskåhl, I. (1995). Sequential treatment of mechanical and chemimechanical pulps with light and heat, a Raman spectroscopic study. *Holzforschung*, *49*, 300–312.

Agarwal, U. P. (1999). An overview of Raman spectroscopy as applied to lignocellulosic materials. In D. S. Argyropoulos (Ed.), *Advances in lignocellulosic characterization* (pp. 209–225). Atlanta, GA: TAPPI Press.

Azizi Samir, M. A. S., Alloin, F., Paillet, M., & Dufresne, A. (2004). Tangling effect in fibrillated cellulose reinforced nanocomposites. *Macromolecules*, *37*, 4313–4316.

Besbes, I., Alila. S., & Boufi, S. Nanofibrillated cellulose from TEMPO-oxidized Eucalyptus fibres: Effect of the carboxyl content. *Carbohydrate Polymers*, in press.

Bhatnagar, A., & Sain, M. (2005). Processing of cellulose nanofiber-reinforced composites. *Journal of Reinforced Plastics and Composites*, *24*(12), 1259–1268.

Czaja, W. K., Young, D. J., Kawecki, M., & Brown, R. M. (2007). The future prospects of microbial cellulose in biomedical applications. *Biomacromolecules*, *8*(1), 1–12.

Dalmas, F., Cavaillé, J. Y., Gauthier, C., Chazeau, L., & Dendievel, R. (2007). Viscoelastic behavior and electrical properties of flexible nanofiber filled polymer nanocomposites. Influence of processing conditions. *Composites Science and Technology*, *67*, 829–839.

De Gennes, P. G. (1976). Scaling concepts in polymer physics. *Journal De Physique Lettres*, *37*, L1.

Edwards, H. G., Farwell, D. W., & Webster, D. (1997). FT Raman microscopy of untreated natural plant fibres. *Spectrochimica Acta Part A: Molecular and Biomolecular Spectroscopy*, *13*, 2383–2392.

Fengel, D. (1971). Ideas on the ultrastructural organization of the cell wall components. *Journal of Polymer Science Part C*, *9*, 383–392.

Fernandes, S. C. M., Oliveira, L., Freire, C. S. R., Silvestre, A. J. D., Pascoal Neto, C., Gandini, A., & Desbriéres, J. (2009). Novel transparent nanocomposite films based on chitosan and bacterial cellulose. *Green Chemistry*, *11*, 2023–2029.

Fukuzumi, H., Saito, T., Wata, T., Kumamoto, Y., & Isogai, A. (2009). Transparent and high gas barrier films of cellulose nanofibers prepared by TEMPO-mediated oxidation. *Biomacromolecules*, *10*(1), 162–165.

Gouyet, J. F. (1992). *Physique et structures fractales*. Paris: Masson.

Habibi, Y., Mahrouz, M., & Vignon, M. R. (2009). Microfibrillated cellulose from the peel of prickly pea fruits. *Food Chemistry*, *115*, 423–429.

Henriksson, M., Henriksson, G., Berglund, L. A., & Lindstrom, T. (2007). An environmentally friendly method for enzyme-assisted preparation of microfibrillated cellulose (nanofibrillated) nanofibers. *European Polymer Journal*, *43*, 3434–3441.

Henriksson, M., Berglund, L. A., Isaksson, P., Lindstrom, T., & Nishino, T. (2009). Cellulose nanopaper structures of high toughness. *Biomacromolecules*, *9*(6), 1579–1585.

Herrick, F. W., Casebier, R. L., Hamilton, J. K., & Sandberg, K. R. (1983). Microfibrillated cellulose: Morphology and accessibility. *Journal of Applied Polymer Science: Applied Polymer Symposium*, *37*, 797–813.

Iwamoto, S., Abe, K., & Yano, H. (2008). The effect of hemicelluloses on wood pulp nanofibrillation and nanofiber network characteristics. *Biomacromolecules*, *9*(3), 1022–1026.

Johnson, R. K., Zink-Sharp, A., Renneckar, S. H., & Glasser, G. W. (2009). A new bio-based nanocomposite: Fibrillated TEMPO-oxidized celluloses in hydroxypropylcellulose matrix. *Cellulose*, *16*, 227–238.

Langford, J. I., & Wilson, A. J. C. (1978). Scherrer after sixty years: A survey and some new results in the determination of crystallite size. *Journal of Applied Crystallography*, *11*, 102–113.

Malainine, M. E., Mahrouz, M., & Dufresne, A. (2005). Thermoplastic nanocomposites based on cellulose microfibrils from Opuntia ficus-indica parenchyma cell. *Composite Science Technologies*, *65*, 1520–1526.

McDougall, G. J., Morisson, I. M., Stewart, D., Weyers, J. D. B., & Hillman, J. R. (1993). Plant fibres: Botany, chemistry and processing for industrial use. *Journal of the Science of Food and Agriculture*, *62*, 1–20.

Nakagaito, A. N., & Yano, H. (2004). The effect of morphological changes from pulp fiber towards nano-scale fibrillated cellulose on the mechanical properties of high-strength plant fiber based composites. *Material Science and Processing*, *78*, 547–552.

Ouali, N., Cavaillé, J. Y., & Perez, J. (1991). Viscoelastic and plastic behavior of multiphase polymer blends. *Plastics Rubber and Composites Processing and Applications*, *16*, 55–60.

Pääkkö, M., Ankerfors, M., Kosonen, H., Nykanen, A., Ahola, S., Osterberg, M., Ruokolainen, J., Laine, J., Larsson, P. T., Ikkala, O., & Lindstro¨m, T. (2007). Enzymatic hydrolysis combined with mechanical shearing and high-pressure homogenization for nanoscale cellulose fibrils and strong gels. *Biomacromolecules*, *8*, 1934–1941.

Saito, T., Hirota, M., Tamura, N., Kimura, S., Fukuzumi, H., Heux, L., & Isogai, A. (2009). Individualization of nanosized plant cellulose fibrils by direct surface carboxylation using TEMPO catalyst under neutral conditions. *Biomacromolecules*, *10*, 1992–1996.

Saito, T., & Isogai, A. (2004). TEMPO-mediated oxidation of native cellulose. the effect of oxidation conditions on chemical and crystal structures of the water-insoluble fractions. *Biomacromolecules*, *5*, 1983–1989.

Saito, T., Nishiyama, Y., Putaux, J. L., Vignon, M., & Isogai, A. (2006). Homogeneous suspensions of individualized microfibrils from TEMPO-catalyzed oxidation of native cellulose. *Biomacromolecules*, *7*, 1687–1691.

Segal, L., Creely, J. J., Martin, A. E., & Conrad, C. M. (1959). An empirical method for estimating the degree of crystallinity of native cellulose using the X-ray diffractometer. *Textile Research Journal*, *29*, 786–794.

Sukjoon, Y., & Jeffery, S. H. (2010). Composites, enzyme-assisted preparation of fibrillated cellulose fibers and its effect on physical and mechanical properties of paper sheet composites. *Industrial & Engineering Chemistry Research*, *49*, 2161–2168.

Syverud, K., & St enius, P. (2009). Strength and barrier properties of MFC films. *Cellulose*, *16*(1), 75–85.

Thygesen, A., Oddershede, J., Lilholt, H., Thomsen, A. B., & Ståhl, K. (2005). On the determination of crystallinity and cellulose content in plant fibres. *Cellulose*, *12*, 563–576.

Turbak, A. F., Snyder, F. W., & Sandberg, K. R. (1983). Microfibrillated cellulose, a new cellulose product: Properties, uses, and commercial potential. *Journal of Applied Polymer Science: Applied Polymer Symposium*, *37*, 815.

Wolfgang, S., & Sanadi, A. R. (2009). Preparation and characterization of cellulose nanofibers from two commercial hardwood and softwood pulps. *Industrial & Engineering Chemistry Research*, *48*, 11211–11219.

Zimmermann, T., Pohler, E., & Geiger, T. (2004). Cellulose fibrils for polymer reinforcement. *Advanced Engineering Materials*, *6*(9), 754–761.